Degradation of High-Power UVC Light-Emitting Diodes via Emission-Activated Nitrogen Vacancy Generation

Chia-Yen Huang, Wen-Hsuan Hsieh, Teng-Li Shao, Chang-Hsien Wu, and Tien-Chang Lu, *Senior Member, IEEE*

***Abstract*—We reported an unexpected power degradation mechanism in high-power ultraviolet C (UVC) light-emitting diodes (LEDs) grown on high-quality AlN templates. The LED underwent an $I = 350$ mA stress for 250 h. After stress, the output power under $I = 350$ mA degraded by 65%. Although the *I–V* curve and *C–V* curve measurements suggested a strong carrier leakage, the electroluminescence (EL) spectrum did not suggest any significant crystal quality degradation in the active region. Cross-sectional transmission electron microscopy (TEM) and energy dispersive X-ray spectroscopy (EDS) mapping revealed new defects nucleated and propagated from the p-GaN/electron blocking layer (EBL) interface. An observable nitrogen loss was introduced to the p-GaN contact layer under EDS. We inferred that the nitrogen desorption was activated by the UVC photon emitted from the active region. The nitrogen vacancies created a continuous leakage path from the active region to the p-electrode via various trap-assisted transport mechanisms.**

***Index Terms*—AlGaN, degradation, GaN, light-emitting diode (LED), trap-assisted tunneling (TAT) ultraviolet C (UVC).**

I. Introduction

AlGaN-BASED deep UV light-emitting diodes (LEDs) have attracted much attention recently for their efficiency and versatility in disinfection application, especially after the outbreak of the COVID-19 pandemic [1], [2], [3], [4]. Significant progress was demonstrated in improving ultraviolet C (UVC) LEDs' light extraction efficiency (LEE) and internal quantum efficiency (IQE). Self-absorbing p-GaN contact layers have been regarded as the limiting bottleneck for LEE. Many studies replaced the p-GaN with an UVC-transparent p-AlGaN contact [5], [6], [7], [8], [9]. The benchmark external quantum efficiency (EQE) for UVC LED with transparent p-AlGaN contact reached 20% under a low current injection [5]. However, the high forward voltage due to the poor electrical contact still hindered the commercialization of UVC LED with p-AlGaN contact. The significant excess of Joule heating by the enhanced forward voltage will facilitate the degradation by material diffusion. Diffusion of point defects into the active region has been regarded as the primary failure mode of ultraviolet B (UVB) and UVC LEDs [10], [11], [12], [13], [14], [15], [16], [17], [18], [19], [20]. For example, magnesium impurity, Ga vacancy (V_{Ga}), and V_{Ga}-related defect complexes diffusing from the electron blocking layer (EBL) and p-GaN were commonly assigned for the new nonradiative recombination centers [10], [11], [12], [13], [14], [15], [16]. Glaab et al. [17] observed a significant hydrogen migration into n-AlGaN after stressing the UVB LED for less than 10 h. Ma et al. [18] observed the electromigration of contact metal toward epitaxy after a 150-h stress. The type of point defects was mostly assigned by the sub-bandgap emission peak in the electroluminescence (EL) spectrum, or the activation energy extracted from deep-level transient spectroscopy. Some studies also revealed that threading dislocations (TDs) served as fast diffusion paths in the degradation process [19], [20].

To reduce the TD density (TDD) of UVC LED epitaxy, high-temperature annealed AlN buffer technology was introduced [21], [22], [23], [24], [25]. The state-of-art TDD of high-quality AlN template on sapphire was reported below 10^8 cm^{-2}, which is superior to most GaN templates on sapphire [23]. Although the thermal strain and lattice-mismatch strain might further nucleate new TDs in subsequent AlN and n-AlGaN epitaxy, those strain-driven defect nucleation can be managed by a high Si-doping in the regrown AlN template [26], [27]. A low TDD in device epitaxy shall not only improve the IQE of LEDs, but also suppress the degradation mechanism assisted by the TDs, theoretically [20]. However, the failure mode of the UVC LED grown low TDD AlN template is rarely discussed. By intuition, adopting a growth template with a lower initial TDD shall favor the device's reliability. In this report, we revealed an unexpected degradation mechanism of UVC LEDs grown on low TDD AlN templates and explained why improving the reliability of UVC LED on these templates could be still challenging. The

Manuscript received 3 February 2023; revised 26 March 2023; accepted 18 April 2023. Date of publication 5 May 2023; date of current version 25 May 2023. This work was supported in part by the National Science and Technology Council under Grant NSTC 111-2628-E-A49-023. The review of this article was arranged by Editor J. Zhang.
(Corresponding author: Chia-Yen Huang.)

The authors are with the Department of Photonics, College of Electrical and Computer Engineering, National Yang Ming Chiao Tung University, Hsinchu 30010, Taiwan (e-mail: cyhuang06@nycu.edu.tw).
Color versions of one or more figures in this article are available at https://doi.org/10.1109/TED.2023.3270130.

Digital Object Identifier 10.1109/TED.2023.3270130

0018-9383 © 2023 IEEE. Personal use is permitted, but republication/redistribution requires IEEE permission.
See https://www.ieee.org/publications/rights/index.html for more information.

Authorized licensed use limited to: National Yang Ming Chiao Tung University. Downloaded on May 13,2025 at 08:28:45 UTC from IEEE Xplore. Restrictions apply.

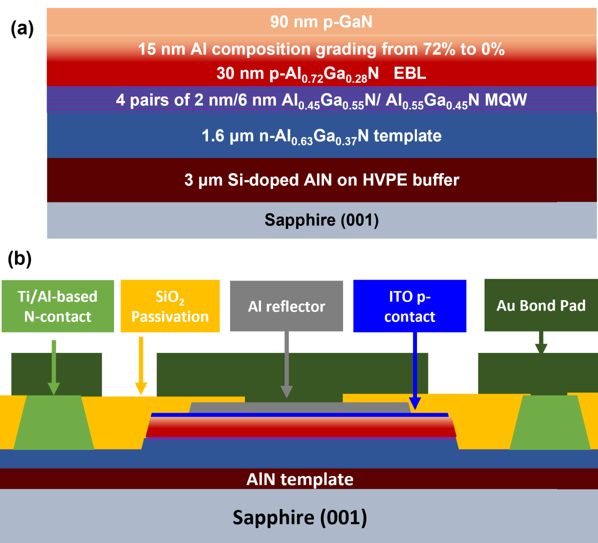

Fig. 1. Schematic illustration of (a) LED epitaxy and (b) flip-chip structure.

failure analysis would provide new insights for UVC LED epilayer design and optimization on low TDD AlN templates, which paves the way toward the realization of a higher total output power, highly efficient, and still robust UVC LED.

II. Device Structure and Experimental Methods

High-quality AlN buffers were deposited by hydride vapor phase epitaxy (HVPE). AlGaN-based LED epi was grown on by TNSC-4000 metal-organic vapor phase epitaxy system on the HVPE buffers. The epi structure above buffer consists of a 3.4 μm Si-doped AlN, a 1.6 μm n-$Al_{0.63}Ga_{0.37}N$, four pairs of 6/2.5 nm $Al_{0.55}Ga_{0.45}N/Al_{0.45}Ga_{0.55}N$ multiple-quantum-wells (MQW), 30 nm p-$Al_{0.75}Ga_{0.25}N$ EBL, 15 nm compositional grading layer (CGL), and 90 nm p-GaN layer. The epitaxial structure is illustrated in Fig. 1(a). The CGL is grown by gradually ramping the group-III precursor flow rates from $Al_{0.72}Ga_{0.28}N$ to GaN under the same growth conditions. Detailed growth conditions and materials characteristics of Si-doped AlN and n-AlGaN can be found in Walde et al. [28]. The epi wafer was fabricated into 1 × 1 mm high power LED flip-chips with Ti/Al-based n-contact and ITO p-contact. SiO_2 was deposited by plasma-enhanced chemical vapor deposition (PECVD) to isolate the n-pad and p-pad. The schematic device structure is illustrated in Fig. 1(b). Five flip-chips with similar initial output power were bonded to the AlN submount for handling, then the submount was bonded to the aluminum-trace printed circuit board (ALPCB) with solder paste for the aging test.

The LEDs were stressed under a continuous 350 mA current injection without external temperature control. After selected aging times, junction temperature (T_j), EL spectrum, and near-field intensity were measured. EL spectrum was measured under two current injection levels, $I = 10$ mA and $I = 350$ mA, for comparison. Current–voltage (I–V) curves and capacitance–voltage (C–V) curves were characterized before bonding and after de-bonding from ALPCB for comparison. After the 250-h stress, the power decay among stressed chips

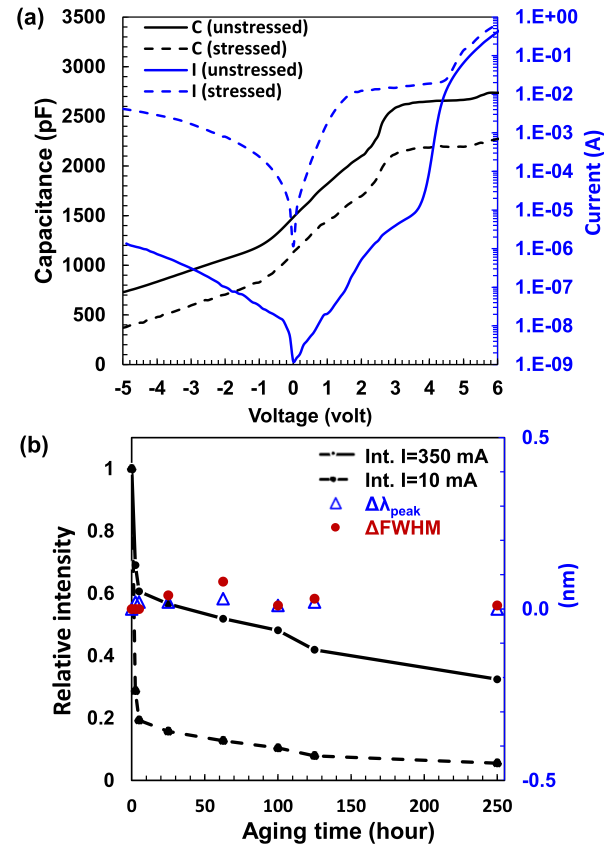

Fig. 2. (a) I–V curves (blue) and C–V curves (black) before (solid line) and after (dashed line) a 250-h stress. (b) Relative EL peak intensity (black) under high current (solid line) and low current (dashed line) at different aging times. Peak wavelength shift (blue triangle) and FWHM variation (red circle) were plotted on the right axis.

under $I = 100$ mA ranged from 53% to 68%. In order to better visualize the failure mode, the chip with the most significant power decay and a nonuniform near-field emission was selected for further failure analysis. Cross-sectional transmission electron microscopy (TEM) characterization and energy dispersive X-ray spectroscopy (EDS) was conducted to probe the crystal quality variation and element re-distribution. In this study, only the I–V, C–V and EL results of the selected die will be shown as the representative.

III. Results and Discussion

The I–V and C–V curves before and after the 250-h stress were plotted in Fig. 2(a). Fig. 2(b) summarized the dependence of relative intensity, EL peak wavelength shift ($\Delta\lambda_{peak}$), and full-width at half-maximum variation (ΔFWHM) with aging time. Before stress, the output power is 60 mW at $I = 350$ mA and ~1 mW at $I = 10$ mA. The peak wavelength is 275 nm and the FWHM is 10.1 nm under $I = 350$ mA. The EL peak intensity dropped rapidly in the first 10 h stress and then degraded slower afterward. The power degradation was more prominent at low current injection ($I = 10$ mA). After a 250-h stress, the EL intensity at 10 mA was only 5% of its original value, while it was still 35% at $I = 350$ mA. The EL intensity degraded significantly, but the EL peak wavelength and FWHM remained invariant. Although point

Authorized licensed use limited to: National Yang Ming Chiao Tung University. Downloaded on May 13,2025 at 08:28:45 UTC from IEEE Xplore. Restrictions apply.

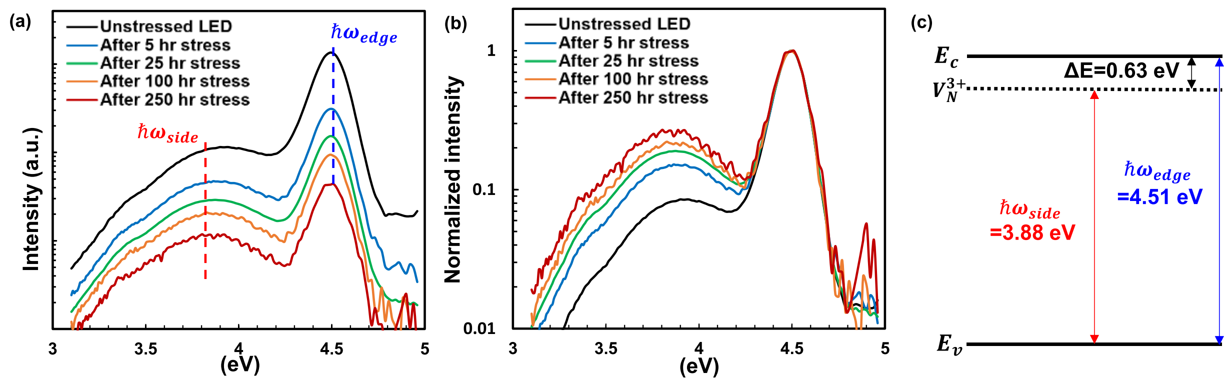

Fig. 3. (a) Raw and (b) normalized EL spectrum under $I = 10$ mA after different aging times. (c) Energy diagram which illustrated the energy level of nitrogen-vacancy between band edges.

defect migration into the quantum well is possible after stress, a significant structural degradation is unlikely. Therefore, the power degradation could not be simply explained by an enhanced non-radiative transition within quantum wells. The variation of the I–V and C–V curves both suggested the generation of strong carrier leakage paths. The leakage current under ideal forward voltage (4.5 V for $\lambda = 275$ nm) enhanced from 10^{-6} to 10^{-2} A after stress. The capacitance also shifted downward by 300–400 pF in a broad voltage range. The I–V and C–V variation implied the power degradation is relevant to the significant carrier losses mechanism in the vicinity of the depletion region.

To identify the type of defect in the active region, the EL spectra under low current injection ($I = 10$ mA) after different aging times were plotted in Fig. 3. Fig. 3(a) plotted the original data while Fig. 3(b) normalized the spectrum to their band edge recombination peak at $\hbar\omega_{\text{peak}} = 4.51$ eV. The peak of parasitic side emission locates in the vicinity of $\hbar\omega_{\text{side}} = 3.88$ eV. The energy difference between $\hbar\omega_{\text{edge}}$ and $\hbar\omega_{\text{side}}$ is 0.63 eV. The degradation of LED cannot be attributed to Mg diffusion into the active region because the activation energy of the Mg acceptor in the quantum well ($Al_{0.45}Ga_{0.55}N$) shall be around 0.3 eV [29]. The sub-bandgap emission was assigned to the recombination between tri-valent nitrogen vacancy donor levels (V_N^{3+}) and valence band edge (E_v) of $Al_{0.45}Ga_{0.55}N$ as depicted in Fig. 3(c). Nakarmi et al. [29] revealed the energy level of V_N^{3+} point defect is ~0.6 eV below the conduction band edge (E_c), which is consistent with the energy separation between $\hbar\omega_{\text{edge}}$ and $\hbar\omega_{\text{side}}$ in Fig. 3. The intensity of band edge emission and side emission both degraded significantly. Although the weight of V_N^{3+}related side emission seems to be enhanced after normalization, it was inadequate to explain the significant overall power degradation. If the power degradation is dominated by the enhanced non-radiative recombination through new V_N^{3+} point defect in QWs, the weight of $\hbar\omega_{\text{side}}$ under low current injection shall eventually surpass $\hbar\omega_{\text{edge}}$ under low current injection. The EL characterization results also suggested that enhanced nonradiative recombination within the quantum well shall not be the dominant mechanism for significant power decay.

The near-field intensity images before and after stress were summarized in Fig. 4(a). Before stress, the emission intensity was uniform over the chip; after a 250-h aging, the emission intensity became much weaker and nonuniform. We selected two regions with a rather bright and dim emission intensity for cross-sectional TEM analysis. Fig. 4(b) is the TEM image of an unprocessed epi-wafer, and Fig. 4(c) and (d) is the TEM image of the brighter and dimmer region after stress, respectively. Before stress, the crystal quality near the active region looks intact, some black spots were observed in the lower interface of p-GaN. We attributed the black spots to the misfit dislocations or local lattice distortion due to the epitaxial strain between p-GaN and its underlayers. It is also possible due to the un-optimized growth conditions or non-ideal ramping scheme while varying the Al composition from 72% (EBL) to 0% (p-GaN). After stress, the MQW crystal quality remained intact under TEM observation, but the whole interface between p-GaN and EBL was darkened. In the dimmer region, the crystal quality deterioration at the interface was more prominent accompanying many dislocations and pipe-like defects in p-GaN only. We inferred the fast degradation below these defect clusters in p-GaN dominated the fast power degradation in the initial stage, and the interfacial degradation in the field contributed to the subsequent slow degradation.

Before stress, the LED demonstrated a low forward voltage due to the high-quality n-AlGaN current injection layer. The forward voltage under $I = 100$ mA was only 4.95 V. However, the measured junction temperature (T_j) was abnormally high for LED on these high-quality templates. The T_j under 100 mA injection was measured to be 125 °C–130 °C, which is higher than that of our other UVC LEDs with a similar epi structure on conventional high TDD AlN templates ($T_j \sim 100$ °C). Therefore, the high T_j of LED on a high-quality template cannot be attributed to neither a higher forward voltage nor a stronger non-radiative recombination in the active region. The enhanced T_j was attributed to the stronger band edge absorption in the p-GaN contact layer under a stronger UVC photon irradiation from quantum wells. The phonons emitted from Shockley–Reed–Hall (SRH) process in the active region will not excite carriers in the p-GaN contact layer to a higher energy band, but the UVC photons will. When the excited carrier in the heavily-doped p-GaN returned to its ground state non-radiatively, it also heated up

Authorized licensed use limited to: National Yang Ming Chiao Tung University. Downloaded on May 13,2025 at 08:28:45 UTC from IEEE Xplore. Restrictions apply.

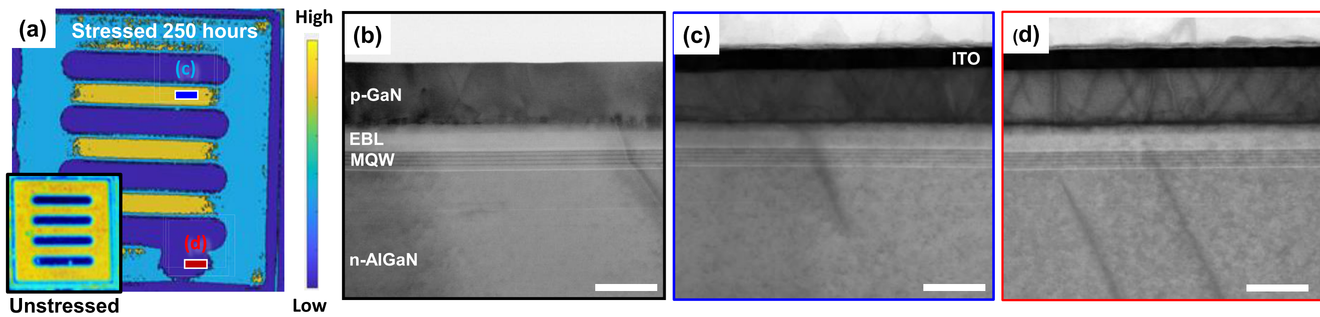

Fig. 4. (a) Relative near-field intensity mapping of a UVC LED before (lower corner) and after 250 h stress taken from a charge-coupled devices (CCD). The intensity is color-coded from low to high on linear scale as shown in the color bar. Blue and red rectangular pointed out where the TEM sample of (c) and (d) was taken. Cross-sectional TEM images from (b) fresh coloaded epi wafer (c) brighter region, and (d) dimmer region of a stressed UVC LED. The white bar in (b)–(d) refers to 100 nm in width.

the device. Therefore, the significantly higher T_j is attributed to the stronger band-edge absorption in the p-contact layer. As a result, UVC LEDs on high-quality AlN templates might degrade even faster if the CGL and p-GaN quality isn't well-optimized.

It is worth noticing that the dislocation density in p-GaN is apparently higher than that in the MQW in Fig. 4(c). Many dislocations in p-GaN are not propagated from the underlayer, but are newly nucleated on the p-GaN growth front. In our previous studies, we revealed that preexisting dislocations are essential for the suppression of drastic TD nucleation in the compressive n-AlGaN growth [27], [28]. If one would like to transfer the low TDD of the AlN template to the subsequent n-AlGaN layer, the compressive strain has to be pre-relaxed without TD nucleation, or the target thickness of n-AlGaN has to be reduced. A similar argument could be applied to the p-GaN contact layer on the UVC LED epilayer up to p-EBL. The p-GaN growth condition and thickness, which is stable on a high TDD UVC LED epi, is not necessarily stable on a low TDD one. In this study, the growth recipe of CGL and p-GaN are directly transplanted from a UVC LED growth recipe which was previously developed on high TDD AlN templates. Although the low TDD was successfully transferred from AlN to MQW after a deliberate strain engineering as shown in Walde et al. [28], the p-GaN contact layer quality could still be deteriorated due to an even larger compressive strain. As a result, the same UVC LED structure could possess a better quality of MQW, but a poorer quality of CGL and p-GaN on the novel low TDD templates. Although the EQE of freshly-made LED is still significantly improved, the promoted degradation from p-GaN became a more critical issue to be overcome.

Fig. 5 showed the EDS element mapping of the TEM sample from Fig. 4(d). Indium (blue), gallium (red), nitrogen (yellow), and oxygen (pink) mapping were shown to identify the components of the LED. In Fig. 5(c), the nitrogen signal appeared to be weaker in the p-GaN than that in its underlayer. In Fig. 4(d), the nitrogen signal is uniform from n-AlGaN to EBL. Therefore, the weaker intensity of nitrogen in p-GaN is unlikely to be an artifact of EDS on III-nitride layers with different alloy compositions. We suggest the decomposition of p-GaN was activated by UVC photons, and then nitrogen vacancies were introduced to p-GaN and its vicinity. We also

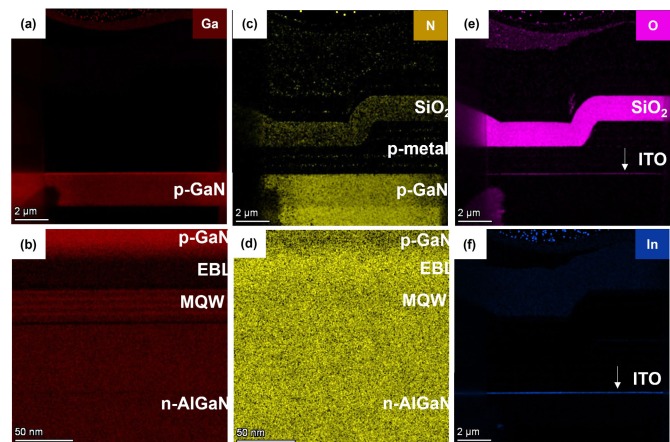

Fig. 5. Element mapping by EDS of (a) Ga on top layers (b) Ga near active region (c) N on top layers (d) N near active region (e) oxygen, and (f) In on top layers of the TEM sample from the aged LED.

observed an unexpected nitrogen trace in the p-metal and PECVD SiO_2 isolation layer, which was attributed to the nitrogen desorption from the p-GaN and CGL. The escaped nitrogen atoms entered the p-metal gradually and accumulated in the SiO_2 layer. Although the p-metal is closer to the p-GaN, the nitrogen signal is stronger in SiO_2 because it is the better accommodation for escaped nitrogen.

The carrier leakage mechanism is illustrated with a band diagram simulation. The band diagram was based on the epilayer structure in Fig. 1 and solved by a 1-D numerical solver developed by Li and Wu [30]. The band diagram was calculated under a forward voltage below turn-on ($V_f = 3.6$ V) as an example and plotted in the vicinity of EBL in Fig. 6. Nitrogen vacancy levels were manually added ~0.6 eV below the E_c to reflect their position in the energy band diagram. According to Fig. 2, background nitrogen vacancies exist in the active region. Since the growth conditions of EBL and active region are similar (N_2 ambient, $T = 1050$ °C, growth rate ~ 0.05 nm/s), nitrogen vacancies shall populate in the EBL region as well. Fig. 5(a) showed how the electron could be transported from the active region to p-GaN via nitrogen vacancies. The electrons are transported from the quantum well to p-GaN by multiple trap-assisted tunneling (TAT) mechanisms, which were commonly observed

Authorized licensed use limited to: National Yang Ming Chiao Tung University. Downloaded on May 13,2025 at 08:28:45 UTC from IEEE Xplore. Restrictions apply.

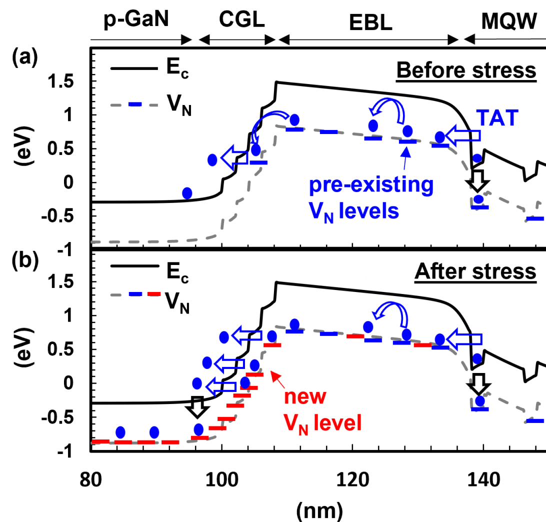

Fig. 6. Schematic energy band diagram of the UVC LED under a 3.6 V forward bias. (a) and (b) Schematically illustrated the nitrogen-vacancy level distribution before and after stress, respectively. Gray dashed lines pointed out the theoretical energy levels for nitrogen vacancies. Blue and red lines marked the preexisting and newly generated nitrogen levels.

in many III-nitride-based optoelectronics and electronics [31], [32], [33], [34], [35]. After stress, a large amount of nitrogen vacancies was generated in the p-GaN and CGL due to the emission-activated nitrogen desorption. The enhanced nitrogen vacancies promoted the aforementioned conduction mechanisms and connected the active region directly to the p-electrode, as illustrated in Fig. 6(b). These donor-like vacancies in the p-side reduced the capacitance of LED, enhanced leakage current via tunneling, and significantly degraded the output power due to the p-n-junction displacement.

IV. Conclusion

In conclusion, we unraveled the UVC LED degradation mechanism by the strong band edge absorption in p-GaN and its interfaces. The emission-activated nitrogen desorption built a strong carrier leakage path between the p-electrode and active region with nitrogen vacancies. This mechanism could be even more prominent for UVC LED grown on high-quality templates due to a stronger UVC photon irradiation under the same current injection. Preexisting defects at the p-GaN/EBL interface might not have a strong effect on the efficiency of freshly-made UVC LEDs, but their strong impact on lifetime still limits the application of high-quality AlN templates to commercial products. If an UVC-transparent and Ohmic p-AlGaN contact layer is not yet available, at least the defect segregation at the p-GaN/EBL interface shall be suppressed. To improve the lifetime of UVC LEDs with a higher output power or a higher IQE, the epitaxial growth of CGL and the p-contact layer shall be carefully dealt with. The p-GaN thickness and CGL ramping strategies also require a thorough re-optimization for UVC LEDs on high-quality AlN templates in order to realize a high total power, highly efficient, while still reliable UVC LED for future commercial application.

Acknowledgment

The authors would like to thank the Industrial Technology Research Institute (ITRI) of Taiwan and SCIOCS Ltd., Japan for the technical support.

References

[1] A. M. Armani, D. E. Hurt, D. Hwang, M. C. McCarthy, and A. Scholtz, "Low-tech solutions for the COVID-19 supply chain crisis," *Nature Rev. Mater.*, vol. 5, no. 6, pp. 403–406, May 2020, doi: 10.1038/s41578-020-0205-1.

[2] F. A. Juarez-Leon, A. G. Soriano-Sanchez, M. A. Rodriguez-Licea, and F. J. Perez-Pinal, "Design and implementation of a germicidal UVC-LED lamp," *IEEE Access*, vol. 8, pp. 196951–196962, 2020, doi: 10.1109/ACCESS.2020.3034436.

[3] M. Bormann et al., "Disinfection of SARS-CoV-2 contaminated surfaces of personal items with UVC-LED disinfection boxes," *Viruses*, vol. 13, no. 4, p. 598, Mar. 2021, doi: 10.3390/v13040598.

[4] S. Liu et al., "Sec-eliminating the SARS-CoV-2 by AlGaN based high power deep ultraviolet light source," *Adv. Funct. Mater.*, vol. 31, no. 7, Feb. 2021, Art. no. 2008452, doi: 10.1002/adfm.202008452.

[5] T. Takano, T. Mino, J. Sakai, N. Noguchi, K. Tsubaki, and H. Hirayama, "Deep-ultraviolet light-emitting diodes with external quantum efficiency higher than 20% at 275 nm achieved by improving light-extraction efficiency," *Appl. Phys. Exp.*, vol. 10, no. 3, Feb. 2017, Art. no. 031002, doi: 10.7567/APEX.10.031002.

[6] Y. Kashima et al., "High external quantum efficiency (10%) AlGaN-based deep-ultraviolet light-emitting diodes achieved by using highly reflective photonic crystal on p-AlGaN contact layer," *Appl. Phys. Exp.*, vol. 11, Nov. 2017, Art. no. 012101, doi: 10.7567/APEX.11.012101.

[7] M. Shatalov et al., "AlGaN deep-ultraviolet light-emitting diodes with external quantum efficiency above 10%," *Appl. Phys. Exp.*, vol. 5, no. 8, Jul. 2012, Art. no. 082101, doi: 10.1143/APEX.5.082101.

[8] H. K. Cho et al., "Enhanced wall plug efficiency of AlGaN-based deep-UV LEDs using Mo/Al as p-contact," *IEEE Photon. Technol. Lett.*, vol. 32, pp. 891–894, 2020, doi: 10.1109/LPT.2020.3003164.

[9] C.-Y. Huang et al., "Efficiency improvement analysis of nano-patterned sapphire substrates and semi-transparent superlattice contact layer in UVC light-emitting diodes," *Appl. Phys. Lett.*, vol. 117, no. 26, Dec. 2020, Art. no. 261102, doi: 10.1063/5.0037588.

[10] D. Monti, M. Meneghini, C. De Santi, G. Meneghesso, and E. Zanoni, "Degradation of UV—A LEDs: Physical origin and dependence on stress conditions," *IEEE Trans. Device Mater. Rel.*, vol. 16, no. 2, pp. 213–219, Jun. 2016, doi: 10.1109/TDMR.2016.2558473.

[11] D. Monti et al., "High-current stress of UV-B (In)AlGaN-based LEDs: Defect-generation and diffusion processes," *IEEE Trans. Electron Devices*, vol. 66, no. 8, pp. 3387–3392, Aug. 2019, doi: 10.1109/TED.2019.2920521.

[12] F. Piva et al., "Stability and degradation of AlGaN-based UV-B LEDs: Role of doping and semiconductor defects," *Microelectron. Rel.*, vols. 100–101, Sep. 2019, Art. no. 113418, doi: 10.1016/j.microrel.2019.113418.

[13] N. Trivellin et al., "Degradation processes of 280 nm high power DUV LEDs: Impact on parasitic luminescence," *Jpn. J. Appl. Phys.*, vol. 58, no. SC, Jun. 2019, Art. no. SCCC19, doi: 10.7567/1347-4065/ab1393.

[14] D. Monti et al., "Defect-related degradation of AlGaN-based UV-B LEDs," *IEEE Trans. Electron Devices*, vol. 64, no. 1, pp. 200–205, Jan. 2017, doi: 10.1109/TED.2016.2631720.

[15] Y.-Z. Wang et al., "Degradation in AlGaN-based UV-C LEDs under constant current stress: A study on defect behaviors," *Appl. Phys. Lett.*, vol. 116, no. 20, May 2020, Art. no. 203501, doi: 10.1063/5.0010540.

[16] J. Glaab et al., "Degradation effects of the active region in UV-C light-emitting diodes," *J. Appl. Phys.*, vol. 123, no. 10, Mar. 2018, Art. no. 104502, doi: 10.1063/1.5012608.

[17] J. Glaab et al., "Degradation of (In)AlGaN-based UVB LEDs and migration of hydrogen," *IEEE Photon. Technol. Lett.*, vol. 31, no. 7, pp. 529–532, Apr. 1, 2019, doi: 10.1109/LPT.2019.2900156.

[18] Z. Ma, H. Cao, S. Lin, X. Li, and L. Zhao, "Degradation and failure mechanism of AlGaN-based UVC-LEDs," *Solid-State Electron.*, vol. 156, pp. 92–96, Jun. 2019, doi: 10.1016/j.sse.2019.01.004.

[19] J. Glaab et al., "Degradation of (InAlGa)N-based UV-B light emitting diodes stressed by current and temperature," *J. Appl. Phys.*, vol. 118, no. 9, Sep. 2015, Art. no. 094504.

Authorized licensed use limited to: National Yang Ming Chiao Tung University. Downloaded on May 13,2025 at 08:28:45 UTC from IEEE Xplore. Restrictions apply.

[20] J. Ruschel et al., "Reliability of UVC LEDs fabricated on AlN/sapphire templates with different threading dislocation densities," *Appl. Phys. Lett.*, vol. 117, Dec. 2020, Art. no. 241104, doi: 10.1063/1.4929656.

[21] H. Miyake, C.-H. Lin, K. Tokoro, and K. Hiramatsu, "Preparation of high-quality AlN on sapphire by high-temperature face-to-face annealing," *J. Cryst. Growth*, vol. 456, pp. 155–159, Dec. 2016, doi: 10.1016/j.jcrysgro.2016.08.028.

[22] C.-Y. Huang et al., "High-quality and highly-transparent AlN template on annealed sputter-deposited AlN buffer layer for deep ultraviolet light-emitting diodes," *AIP Adv.*, vol. 7, no. 5, May 2017, Art. no. 055110, doi: 10.1063/1.4983708.

[23] D. Wang, K. Uesugi, S. Xiao, K. Norimatsu, and H. Miyake, "High-quality AlN/sapphire templates prepared by thermal cycle annealing for high-performance ultraviolet light-emitting diodes," *Appl. Phys. Exp.*, vol. 14, Feb. 2021, Art. no. 035505, doi: 10.35848/1882-0786/abe522.

[24] S. Walde, S. Hagedorn, and M. Weyers, "Impact of intermediate high temperature annealing on the properties of AlN/sapphire templates grown by metalorganic vapor phase epitaxy," *Jpn. J. Appl. Phys.*, vol. 58, Apr. 2019, Art. no. SC1002, doi: 10.7567/1347-4065/ab0cfc.

[25] N. Susilo et al., "Improved performance of UVC-LEDs by combination of high-temperature annealing and epitaxially laterally overgrown AlN/sapphire," *Photon. Res.*, vol. 8, pp. 589–594, Apr. 2020, doi: 10.1364/PRJ.385275.

[26] A. Mogilatenko, S. Walde, S. Hagedorn, C. Netzel, C.-Y. Huang, and M. Weyers, "Impact of Si doping on dislocation behavior in MOVPE-grown AlN on high-temperature annealed AlN buffer layers," *J. Appl. Phys.*, vol. 131, no. 4, Jan. 2022, Art. no. 045702, doi: 10.1063/5.0073076.

[27] C.-Y. Huang et al., "Overcoming the excessive compressive strain in AlGaN epitaxy by introducing high Si-doping in AlN templates," *Jpn. J. Appl. Phys.*, vol. 59, no. 7, Jun. 2020, Art. no. 070904, doi: 10.35848/1347-4065/ab990a.

[28] S. Walde et al., "High-quality AlGaN epitaxy on lattice-engineerable AlN template for high-power UVC light-emitting diodes," *Acta Mater.*, vol. 226, Mar. 2022, Art. no. 117625, doi: 10.1016/j.actamat.2022.117625.

[29] M. L. Nakarmi, N. Nepal, J. Y. Lin, and H. X. Jiang, "Photoluminescence studies of impurity transitions in Mg-doped AlGaN alloys," *Appl. Phys. Lett.*, vol. 94, no. 9, Mar. 2009, Art. no. 091903, doi: 10.1063/1.3094754.

[30] C.-K. Li and Y.-R. Wu, "Study on the current spreading effect and light extraction enhancement of vertical GaN/InGaN LEDs," *IEEE Trans. Electron Devices*, vol. 59, no. 2, pp. 400–407, Feb. 2012, doi: 10.1109/TED.2011.2176132.

[31] Q. Shan et al., "Transport-mechanism analysis of the reverse leakage current in GaInN light-emitting diodes," *Appl. Phys. Lett.*, vol. 99, no. 25, Dec. 2011, Art. no. 253506, doi: 10.1063/1.3668104.

[32] M. A. der Maur, B. Galler, I. Pietzonka, M. Strassburg, H. Lugauer, and A. D. Carlo, "Trap-assisted tunneling in InGaN/GaN single-quantum-well light-emitting diodes," *Appl. Phys. Lett.*, vol. 105, no. 13, Sep. 2014, Art. no. 133504, doi: 10.1063/1.4896970.

[33] Y. Kajikawa, "Hall factor for hopping conduction in n- and p-type GaN," *Phys. Status Solidi C*, vol. 14, nos. 1–2, Nov. 2016, Art. no. 1600129, doi: 10.1002/pssc.201600129.

[34] A. Muhin et al., "Vertical conductivity and Poole–Frenkel-ionization of Mg acceptors in AlGaN short-period superlattices with high Al mole fraction," *Appl. Phys. Lett.*, vol. 117, no. 25, Dec. 2020, Art. no. 252101, doi: 10.1063/5.0027336.

[35] R. Swain, K. Jena, and T. R. Lenka, "Modeling of forward gate leakage current in MOSHEMT using trap-assisted tunneling and Poole–Frenkel emission," *IEEE Trans. Electron Devices*, vol. 63, no. 6, pp. 2346–2352, Jun. 2016, doi: 10.1109/TED.2016.2555851.

Authorized licensed use limited to: National Yang Ming Chiao Tung University. Downloaded on May 13,2025 at 08:28:45 UTC from IEEE Xplore. Restrictions apply.